Radiation Environment Monitor

P. Bühler, S. Ljungfelt, A. Mchedlishvili, N. Schlumpf, A. Zehnder
Paul Scherrer Institute, CH–5232 Villigen PSI

L. Adams, E. Daly, R. Nickson
ESA/ESTEC, NL–2200 AG Noordwijk

September 24, 1999

Abstract

The Radiation Environment Monitor (REM) is a modular, programmable monitor for the radiation environment on spacecrafts. REM accumulates differential linear energy transfer spectra of two independent silicon detectors with different shieldings. The instrument is sensitive to protons with energies between 30 MeV and 600 MeV and to electrons with energies between 1 MeV and 10 MeV.
During the year 1994 two REM instruments were launched into space, one into a Geostationary Transfer Orbit and one into a Low Earth Orbit. Both instruments are working well and provide simultaneous information on the space radiation environment of different orbits.
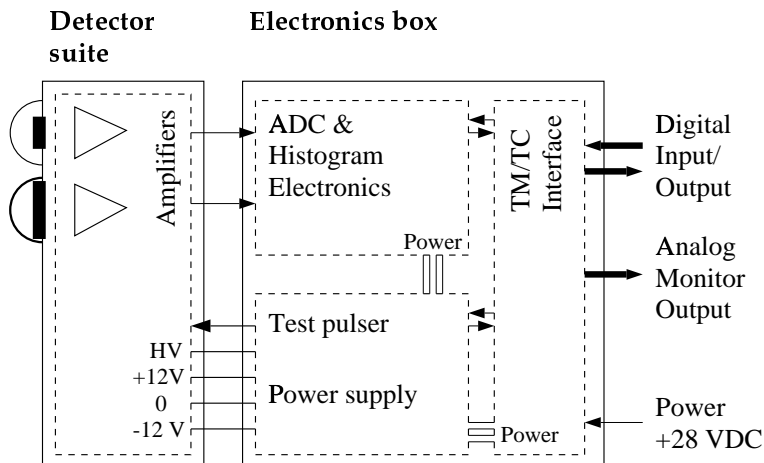
Figure 1: Layout of the detector suite and electronics box. The detector suite contains the two silicon detectors and the analog readout electronics. The electronics box contains the A/D conversion, data processing, and control electronics and the communication interface to the on-board computer.

1 Introduction

The Radiation Environment Monitor (REM) is an instrument for monitoring the radiation environment on spacecrafts. The motivation for its development was to provide a simple instrument of low weight and low power consumption, but which is nevertheless versatile, providing temporal data and some degree of discrimination, both in particle species and energy.

REM is designed to measure the flux of protons with energies between 30 and 600 MeV and electrons with energies above 1 MeV. The REM contains two solid state detectors measuring the differential linear energy transfer of charged particles. Two detectors with different areas and shielding configuration are used making them selective sensitive to different ranges of particle properties. During 1994 two REM instruments were launched, one aboard the UK STRV-B satellite into a Geostationary Transfer Orbit (GTO) and one on the Russian MIR space station into a Low Earth Orbit (LEO). Both instruments are planned to be operational until at least the end of 1995.

The paper is organized as follows. In section 2 we give a description of the REM detectors. The response of the instrument to protons and electrons is expressed in form of geometric factors which are discussed in section 2.1. Data reduction consists of two steps: deadtime correction and extraction of the spectral information. The applied methods are outlined in section 3. In section 4 we demonstrate the in–flight performance of the REM instruments in space.

2 REM instrument description

The REM instrument includes two modules, the detector suite and the electronics box. The layout of the two units is shown in figure 1. The detector suite contains two solid state detectors and the analog readout electronics. Its physical dimensions are 13 × 10 × 8 cm and it has a weight of approximately 1 kg. The electronics box contains the A/D conversion and the digital data processing electronics and provides the interface of the instrument with spacecraft telemetry and power. This unit measures 20 × 16 × 8 cm and weights 1.8 kg.
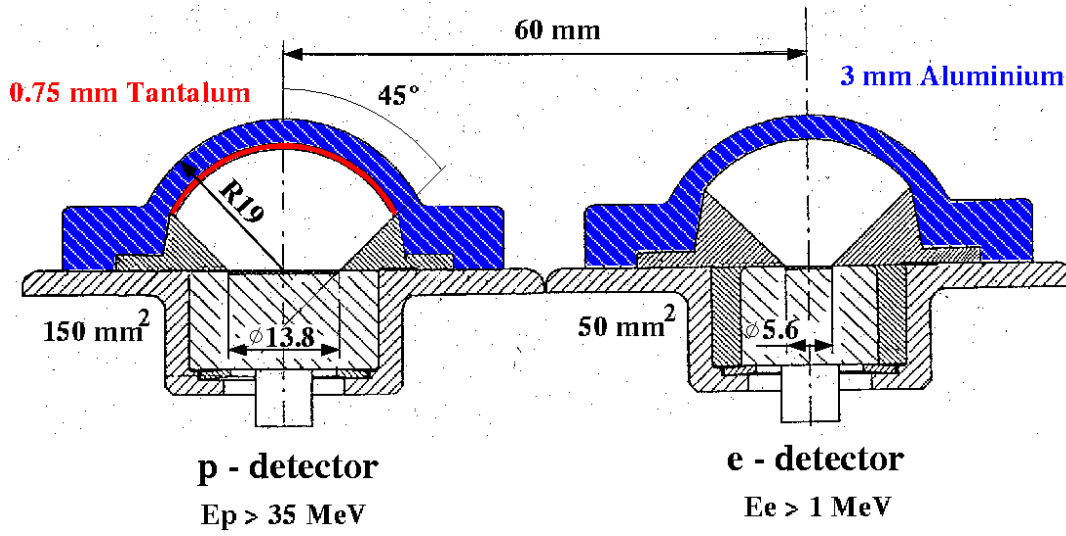
Figure 2: Cutaway view of the two REM silicon detectors and their shielding. Both detectors are covered with a spherical dome of aluminium. The p–detector is equipped with an additional tantalum layer preventing electrons from penetrating the detection volume. The main aperture is defined by an aluminium cone with an opening angle of $\pm 45°$.

The two modules are interconnected via two cables. The maximum total power consumption is less than 5 W. The detector suite contains two independent, totally depleted silicon surface barrier detectors, measuring the linear energy transfer (LET) of charged particles (protons, electrons, ions) passing through. The employed detectors are from EG&G (B–series). A cutaway view of the detector head is shown in figure 2.

Both detectors are covered with a spherical dome of aluminium. One detector has an additional shielding of tantalum. Whereas the detector without tantalum (in the following referred to as e–detector) sees protons as well as electrons, the extra tantalum of the other detector reduces the penetration of electrons in the relevant energy range (1 – 10 MeV) significantly and makes this detector better at monitoring protons (in the following referred to as p–detector). The thickness of the shielding has been determined by Monte Carlo simulations, using realistic space environment inputs. They were optimized for particle discrimination and processable count rates (less than $2 \cdot 10^4$ Hz). The characteristic detector sizes and the implemented shieldings are summarized in table 1. The shielding materials and thicknesses define the lower energy thresholds E_{th} for particles to penetrate the shielding which also are given in table 1.

The main aperture is defined by an aluminium cone, mounted on top of each diode. The opening angle is $\pm 45°$. However, the backside of the detectors is, except by the detector suite housing and the spacecraft, not specially protected such that particles from the backside also contribute to the detections.

The charge pulses produced by the particles passing through the silicon diodes are measured using charge sensitive pre–amplifier and 12–bit ADCs. In order to reduce the data amount the ADC outputs are compressed into 16-bin histograms. The compression function is defined by a programmable ROM thus allowing mission dedicated binnings. The binning used in the STRV–REM and MIR–REM is described in table 2. The deposited energies are given in MIPS of protons (1 MIPS = 0.39 keVμm^{-1} or 1.6 MeVg^{-1}cm^2 in silicon). The corresponding values for

Table 1: Properties of REM detectors aboard the STRV–satellite and the MIR station.

Mission	Detector	Sensitive detector area [mm^2]	Thickness of silicon diode [μm]	Shielding [mm, material]	Threshold energy E_{th} [MeV] electrons	protons
STRV	p	150	298	3.0, aluminium 0.75, tantalum	2.6	35.0
	e	50	310	3.0, aluminium	1.4	24.0
MIR	p	150	330	3.0, aluminium 0.75, tantalum	2.6	34.0
	e	25	267	0.71, aluminium	0.7	10.0

electrons are obtained by multiplication with a factor 1.1. Note that the detectors are sensitive to energy deposits below the minimum loss of charged particles up to 1000 times the energy loss of minimum ionizing particles.

Data is successively accumulated during typically 100 seconds. The two resulting 16-bin histograms are transferred to the spacecraft memory. Each accumulation is followed by a reading of the house keeping data which comprises the high–voltage and electronic–supply–voltage values and the levels of four temperature sensors placed at critical points in the detector suite and electronics box.
A built–in test pulser allows to artificially induce charge pulses at the input of the pre–amplifiers at a predefined rate. This pulser is used to check for proper functioning of the detector electronics and for dead–time determination.

2.1 Detector response

The response of the instrument to incident particles is mainly defined by the shielding and the differential energy release dE/dx(E) in silicon. The shielding determines the lower energy cut-offs, whereas the energy dependence of the LET function determines the energy sensitivity of the detector. Due to the variation of the energy loss of protons in silicon [1] in the energy range between 10 and 10^3 MeV the incident energy of the protons is measured. On the other hand the energy loss curve of electrons in silicon [2] is practically flat between 1 and 10 MeV and therefore the energy of the electrons is only poorly resolved. However, combining the measurements of both detectors allows to determine the hardness of the electron spectra.
The energy resolution is in addition limited by the large acceptance angle. The track length through the silicon varies with the angle of incidence which produces a smearing of the energy response.
We express the energy response of each REM detector by its geometric factors per histogram bin $G_k(E, \alpha, i)$. $G_k(E, \alpha, i)$ is an area, expressed in cm^2, which's size is proportional to the probability for an incident particle of species k (p, e, ions) with energy E and angle of incidence α to be detected in histogram bin i. In the following the index i will run from 1 to 32, where bins 1 to 16 are the p-detector bins and bins 17 to 32, the e-detector bins.
The geometric factors were determined by calibration measurements and Monte Carlo simulations. At the Proton Irradiation Facility (PIF) [3] at Paul Scherrer Institute the detector suite was irradiated with protons in the energy range from 45 MeV to 300 MeV [4],[5] and at the Betatron of the University of Zürich with 1 to 10 MeV electrons [6] for several angles between

4

Table 2: Histogram compression function applied in the STRV–REM and MIR–REM instruments. The deposited energies are given in MIPS of protons.

Histogram bin	ADC output range	Deposited energy [MIPS] p–detector	Deposited energy [MIPS] e-detector
1	1	0.5 − 0.7	0.2 − 0.4
2	2	0.7 − 1.0	0.4 − 0.7
3	3 − 6	1.0 − 1.9	0.7 − 1.6
4	7 − 8	1.9 − 2.4	1.6 − 2.1
5	9 − 10	2.4 − 2.8	2.1 − 2.5
6	11 − 12	2.8 − 3.3	2.5 − 3.0
7	13 − 15	3.3 − 4.0	3.0 − 3.7
8	16 − 19	4.0 − 5.0	3.7 − 4.6
9	20 − 23	5.0 − 5.9	4.6 − 5.6
10	24 − 30	5.9 − 7.6	5.6 − 7.2
11	31 − 42	7.6 − 10.4	7.2 − 10.0
12	43 − 79	10.4 − 19.1	10.0 − 18.6
13	80 − 275	19.1 − 65.3	18.6 − 64.2
14	276 − 727	65.3 − 171.4	64.2 − 169.7
15	728 − 4000	171.4 − 942.6	169.7 − 934.0
16	4001 − 4095	> 940	> 930

$0°$ and $180°$. The measurements were subsequently simulated with the GEANT code developed at CERN [7] and an excellent agreement was found. After computer code and geometric model had been proven to be sufficiently accurate, extensive simulations of the complete instruments including carrying satellite/space station were performed [8]. For this purpose particles were assumed to be isotropically distributed in space. Thus the resulting geometric factors represent an average over all incident angles ($G_k(E,i)$). The results for the STRV–REM are shown in figure 3.

There are some particular features to note:

The distribution of G_p among the histogram bins has two maxima. They evolve parallel from small bin numbers at high energies to large bin numbers at low energies. The two maxima originate from particles incident from the front (lower maxima) and from the back (higher maxima), respectively.

Electrons with energies below 4 MeV are efficiently absorbed in the tantalum of the p–detector shielding. This implies that for electrons with large energies the count rate ratio of the e− to p–detector is ≈ 1 whereas this ratio is $\gg 1$ at small electron energies. This effect provides some information on the hardness of the incident electron spectrum.

Although G_e decreases rapidly with smaller energies it must be taken into account because the electron flux in the radiation belts is known to steeply increase in this energy range.

The relative contribution in histogram bins 1 and 2 is largest for electrons in the the p–detector. These low energy events are caused by electrons producing bremsstrahlung in the aluminium dome. In the tantalum dome some of these bremsstrahlung photons produce photo electrons which contribute to the detections in the lowest p–detector channels. However the first two bins are sensitive to gain variations of the amplifiers and are mainly used to monitor these drifts.
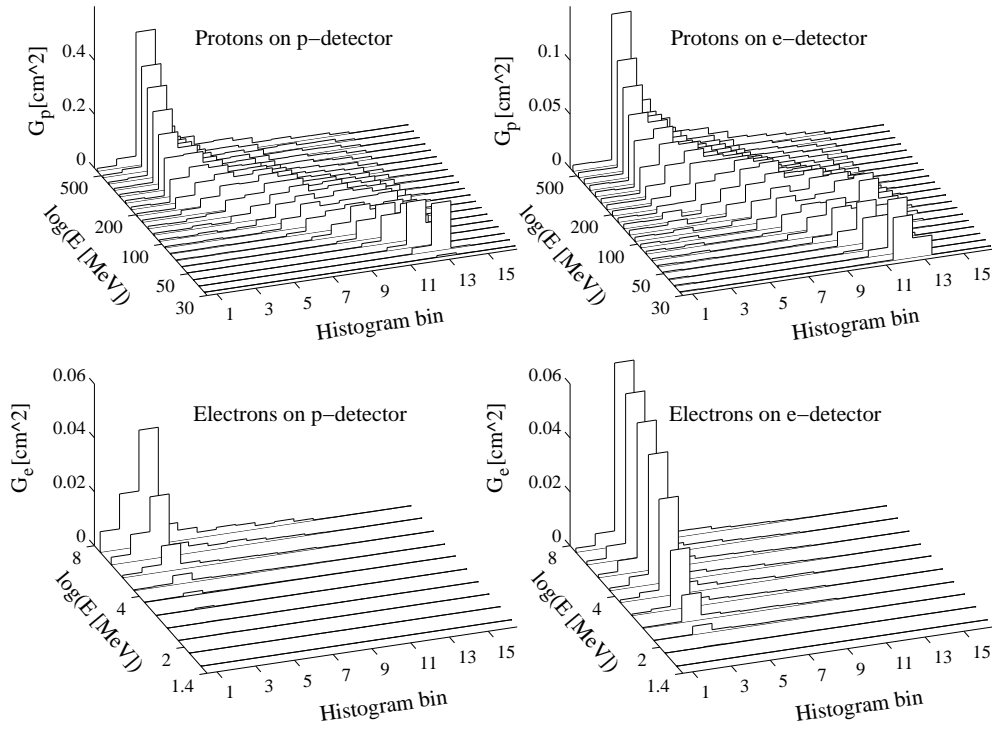
Figure 3: Detector response matrix $G_k(E,i)$ of the STRV-REM detectors for electrons and protons.

The contribution of protons and electrons in the two highest histogram bins is negligibly small. These channels are expected to contain the detections of ions. In–flight measurements however show no significant count rates in these channels.

The sensitivity of the REM detectors for the shape of the incident proton energy spectrum is demonstrated in figure 4. The two histograms are the result of a simulation of protons with a power law spectrum, $f_p(E) = A \cdot E^{-\gamma}$, with $\gamma = 1.3$ and $\gamma = 1.7$, respectively, values typical for protons in the inner radiation belt. The soft spectrum ($\gamma=1.7$) contributes more to the count rate in the high bins, whereas the hard spectrum ($\gamma=1.3$) contributes most to the low–bin count rates.

In section 3 we will discuss a method to calculate the incident particle energy spectra from the measured histograms using the geometric factors.

3 Data reduction

The aim of the data reduction is to extract the spectral information about the environmental protons and electrons from the accumulated histograms. The data reduction procedure consists of two steps: first the raw data has to be corrected for deadtime effects and then the corrected data are deconvoluted.

The deadtime t_D is regularly measured with the built–in test pulser and is interpolated for each data accumulation.
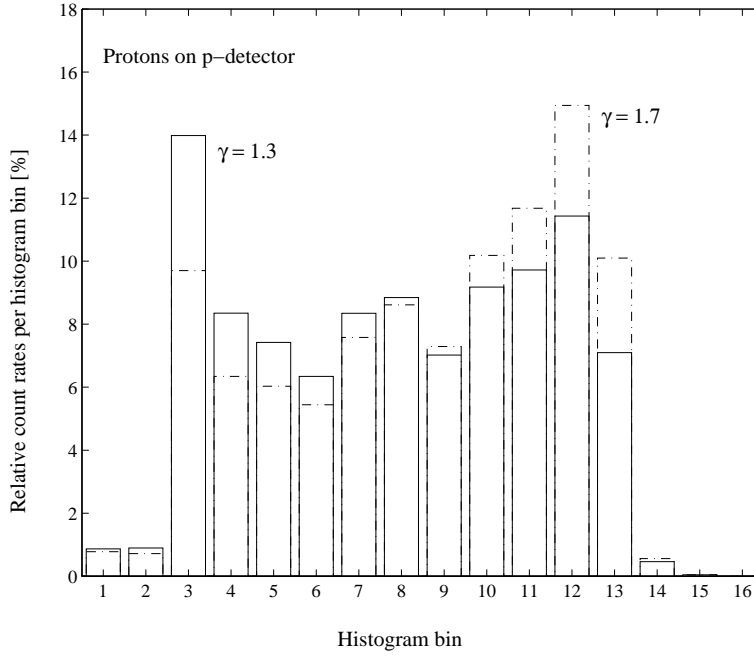
Figure 4: Simulated response in the p-detector for protons with a power law energy spectrum $f = A \cdot E^{-\gamma}$ with γ=1.3 (bold line) and 1.7 (dashed line), respectively. The harder spectrum ($\gamma = 1.3$) contributes most to low histogram bins, whereas the softer spectrum ($\gamma = 1.7$) contributes more to high bins.

The corrected count rates per histogram bin c_i are obtained with

$$c_i = c_i^0 \cdot (1 - t_D)^{-1} \tag{1}$$

where c_i^0 is the detected count rate per histogram bin.

The deadtime corrected count rates are related to the omnidirectional proton and electron fluxes (f_p and f_e) and the geometric factors of the instrument by

$$c_i = \int_0^\infty dE \cdot f_p(E) \cdot G_p(E, i) + \int_0^\infty dE \cdot f_e(E) \cdot G_e(E, i) \tag{2}$$

where f_k is given in $\mathrm{HzMeV^{-1}cm^{-2}}$.

The particle energy spectra are deduced using equation (2). Therefore the spectra have to be parametrized in some manner and the characterizing parameters found by fitting equation (2) to the observed count rates c_i. Because of the limited energy sensitivity of the instrument the number of fittable parameters and with that the complexity of the model spectra is restricted. The problem can be reduced to a linear one by approximating the spectra by step–like functions: the particle energy spectra are supposed to be piece–wise constant in selected energy intervals. Equation (2) then transforms to

$$c_i = \sum_{m=1}^{N_p} f_{p,m} \cdot \int_{E_{p,m}^{min}}^{E_{p,m}^{max}} dE \cdot G_p(E, i) + \sum_{n=1}^{N_e} f_{e,n} \cdot \int_{E_{e,n}^{min}}^{E_{e,n}^{max}} dE \cdot G_e(E, i) \qquad (3)$$

$$= \sum_{m=1}^{N_p} f_{p,m} \cdot D_{p,m}(i) + \sum_{n=1}^{N_e} f_{e,n} \cdot D_{e,n}(i)$$

with

$$D_{k,l}(i) = \int_{E_{k,l}^{min}}^{E_{k,l}^{max}} dE \cdot G_k(E, i)$$

N_p is the number of energy intervals the proton spectrum has been divided up and $f_{p,m}$ is the proton flux level in the energy interval $E_{p,m}^{min}$ and $E_{p,m}^{max}$ (correspondingly for electrons: N_e, $f_{e,n}$, $E_{e,n}^{min}$, and $E_{e,n}^{max}$). The linear equation can be written as a matrix equation

$$\vec{c} = \mathcal{D} \times \vec{f} \qquad (4)$$

where $\vec{c}$ is a 32-element vector containing the deadtime corrected count rates, $\vec{f}$ is a $N_p + N_e$ element vector of all proton and electron flux levels, and $\mathcal{D}$ a $(N_p + N_e) \times 32$ element matrix containing the geometric factors integrated over energy in the ranges $E_{k,l}^{min}$, $E_{k,l}^{max}$. Equation (4) is a so–called linear programming for which dedicated solution algorithms exist [9].

4 REM in–flight performance

On June 17, 1994 the two UK Space Technology Research Vehicles STRV-1A and STRV-1B were launched into space with the Ariane rocket 44LP/V64 [10]. Among other experiments [11] there is a REM instrument aboard the STRV-1B satellite. In the middle of September, 1994 a second REM was shipped to the Russian manned space station MIR and was subsequently mounted on the outside of the space station by a cosmonaut. Both instruments are working well since their first switch–on and are delivering data regularly. The STRV satellite was designed for a nominal lifetime of 12 month. Due to the good functioning of REM the mission will be prolongated by an additional year, such that STRV-REM data can be expected until the middle of year 1996. MIR–REM forms part of the EUROMIR-95 experiment. Its operation is guaranteed for one year until October, 1995.

4.1 STRV–REM data

The STRV-1B satellite was launched into a geostationary transfer orbit (GTO) with apogee and perigee altitudes of 300 and 36000 km, respectively and a period of approximately ten hours. The orbit inclination is 7°.
STRV-1B is a spin stabilized satellite with a spinning rate of $\approx$ 6.5 rpm. The spinning axis is controlled to be perpendicular to the sun-satellite axis. During each orbit the satellite passes through both earth radiation belts and covers L–shell values from 1 to 7. McIlwain's L–shell parameter is a length expressed in earth radii R_E; it is based on the geomagnetic field and is approximately equal to the distance from the center of the earth to the equatorial crossing of the magnetic field line.
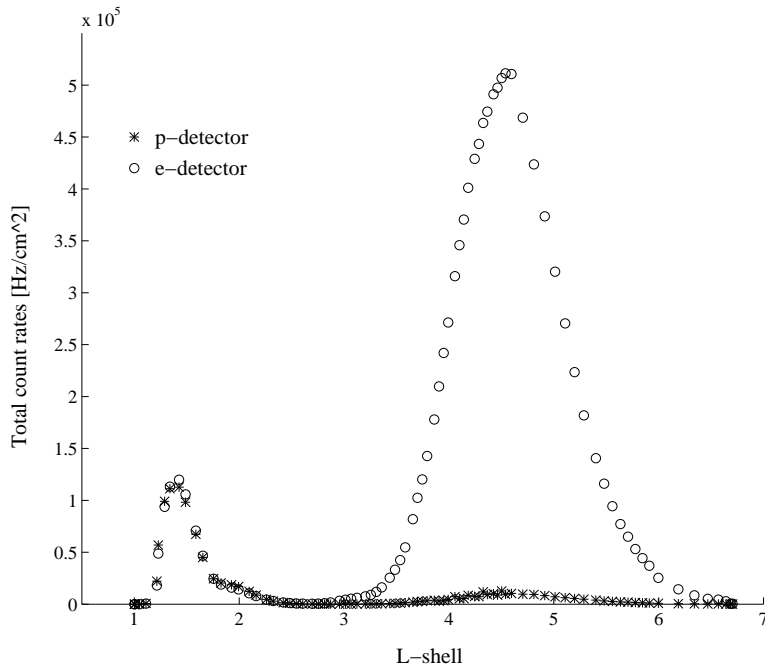
Figure 5: Total deadtime corrected count rates versus L–shell. The data were taken on December 6, 1994 by the STRV-REM instrument. The low count rates in the p–detector compared to the e–detector at L–shell values between 3.5 and 6 show the efficient discrimination of electrons in the p–detector.

The operation of the REM on the STRV is controlled by processing tables which are uploaded from ground and define start and stop times and the sequence of accumulation times. Accumulation times are short during the passage through the radiation belts and longer during the passage at perigee.

The length of an uninterrupted observation session is limited by the onboard data storage capacity to a maximum of two contiguous orbits. Since July 1994 the observation time per month has been continuously increased from 10% to 50% in November 1994 and lies since then between 50% and 70% of the available time.

The course of the count rates over one orbit is characterized by the passage through the radiation belts. In figure 5 the total deadtime corrected count rates ($\sum_{i=1}^{16} c_i$), normalized to the detector area, are plotted versus the L–shell parameter [12] for an exemplary orbit on December 6, 1994. The fact that the outer belt ($3.5 < L < 6$) is less expressed in the p–detector ($*$) than in the e–detector ($\circ$) shows that the outer radiation belt is dominated by electrons, as expected.

In figure 6 three deconvoluted proton spectra are shown taken during the passage through the inner radiation belt (L=1.3, 1.5, and 1.8) on December 6, 1994. The step-like functions are the non-negative least square solutions of the linearized problem (equation (4)) whereas the straight lines with circles are the results of a fit with equation (2), assuming the proton and electron spectra to follow a power law. In order to separate the curves in the figure, the spectra at L=1.3 and L=1.8 are multiplied with a factor 10 and 0.5, respectively. The agreement of the two methods is very good. The shown results demonstrate the softening of the proton spectrum with increasing distance from earth. For the linearized method the energy limits $E_{k,l}^{min}$, $E_{k,l}^{max}$ have been chosen to be {24, 45, 90, 170, 315, 600} MeV for protons and {1.4, 2, 10} MeV for electrons.
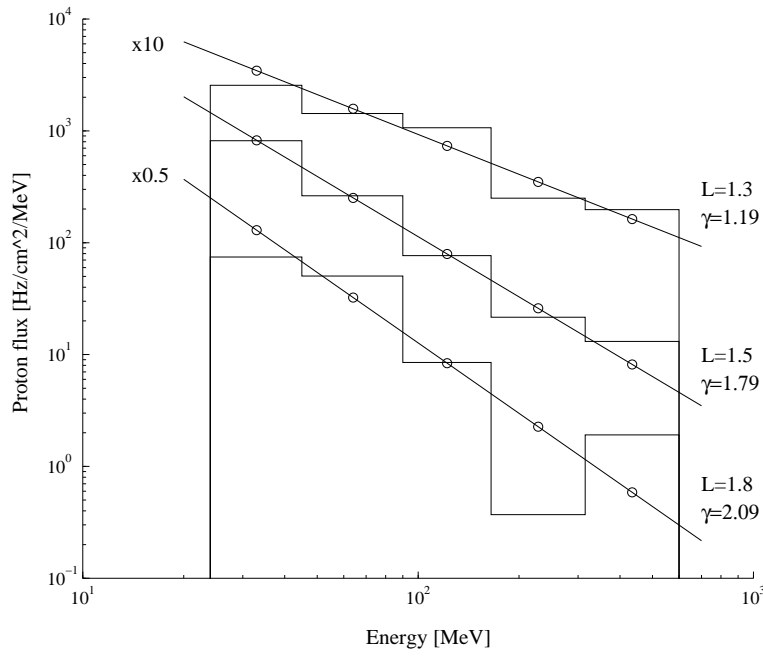
Figure 6: Measured proton spectra in the inner radiation belt. The step–like functions are the solution of the linearized equation (4) whereas the straight lines with circles are the result of a fit with equation (2), assuming the proton and electron spectra to follow a power law. The proton spectra get softer (increasing power index γ) with larger distance from earth.

The limited energy resolution for electrons does not allow more than two energy intervals. However, with the two resulting electron flux levels $f_{e,1}$ and $f_{e,2}$ variations of the spectral hardness can be monitored. In figure 7 the two flux levels are plotted versus L for the passage through the outer radiation belt on November 19, 1994. The steepening of $f_{e,1}$ relative to $f_{e,2}$ at small and large L values, is an indication of the hardening of the electron spectrum at the inner and outer edge of the outer radiation belt.
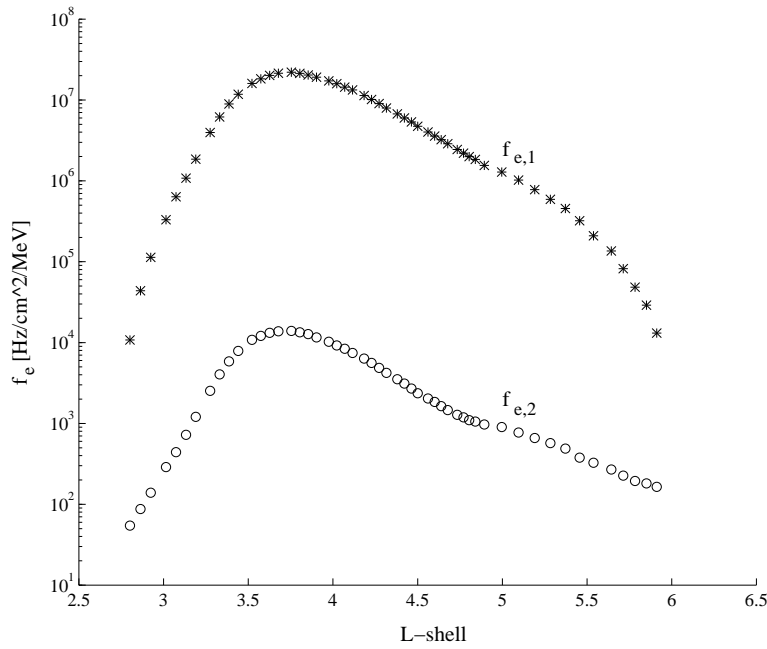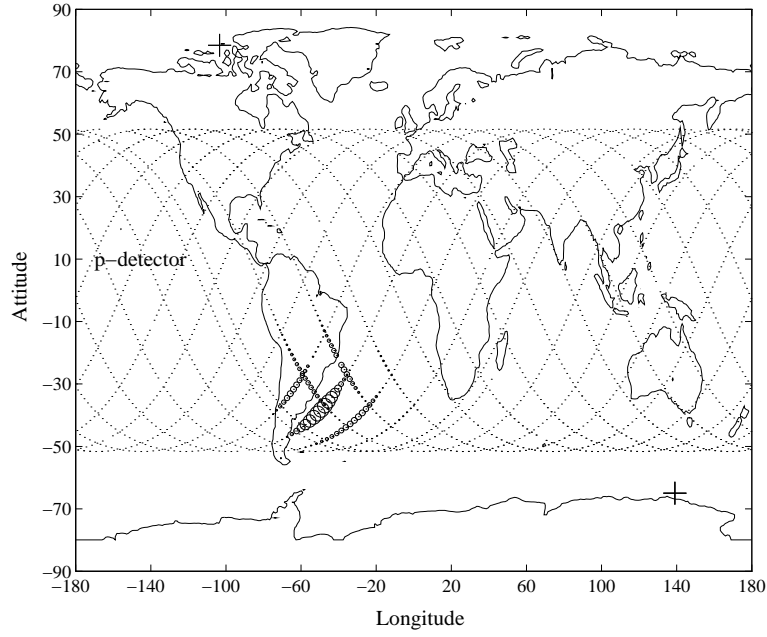
Figure 7: Differential electron flux measured on November 19, 1994 during the passage of STRV–REM through the outer radiation belt. $f_{e,1}$ and $f_{e,2}$ are the differential fluxes between 1.4 and 2.0 MeV and 2.0 and 8.0 MeV, respectively, and were obtained by solving the linearized equation (4).
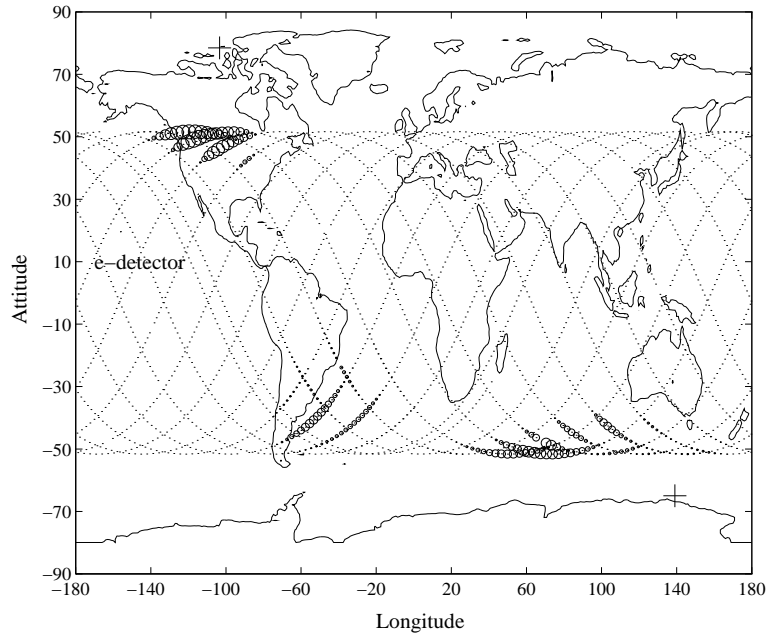
4.2 MIR–REM data

The MIR station orbits the earth every 90 minutes on a nearly circular orbit with an inclination of $52°$ in an altitude of ≈ 400 km. The range of L values covered reaches from below 1 up to 6.5.

The MIR–REM is programmed to accumulate data with pre–defined accumulation times of 32 seconds. Every approximately 24 hours the data is downloaded. Since November 1994 REM was switched off only two times for a period of several days, but otherwise was working regularly. The return factor lies between 60% and 70%.

The MIR-REM measurements are dominated by the high energy protons in the South Atlantic Anomaly (SAA) and electrons at large geomagnetic latitudes which are brought to low altitudes by magnetic field lines. In figure 8 the total deadtime corrected count rates in p– and e–detector measured at December 10, 1994 are plotted as a function of satellite position. The sizes of the markers (○) are proportional to the count rates and the dotted lines show the MIR trajectory. The protons of the SAA are detected in both detectors whereas the electrons at high latitudes only show up in the e–detector.

a)

b)

Figure 8: MIR–REM count rates measured on December 10, 1994: a) p-detector, b) e-detector. The sizes of the markers (○) are proportional to the count rates and the dotted lines show the trajectory of the MIR station. The protons of the SAA are detected in both detectors whereas the electrons at high latitudes only show up in the e–detector.

5 Outlook / Conclusion

In the first ten month of operation REM has proved to be a reliable instrument for the monitoring of the space radiation environment. The accumulated data will be useful for the determination of the severity of the radiation environment for satellites on the two specific orbits which is an important input for the design of future space missions.

On the other hand the obtained information will also contribute to investigations of the physics of trapped particles in the earth magnetosphere. A first look through the data shows a highly dynamical behaviour of the radiation environment which is not described with the actual models. The frequently cited AP–8 and AE–8 models of NASA [13],[14] are 20 years old and need updating and improvement.

The unique situation of simultaneous measurements on different orbits allows to study correlations and dependencies. Together with geomagnetic, solar, and other satellite data the temporal and spatial development of the particle fluxes will be investigated. Their understanding is crucial for a reliable forecast of the space weather.

References

[1] Janni, J.F. Proton range–energy tables, 1 keV – 10 GeV. *Atomic Data and Nuclear Data Tables*, 27:147, 1982.

[2] Pages, L., Bertel, E., Joffre, H., and Sklaventitis, L. Energy loss and bremsstrahlung yield for 10 keV to 100 MeV electrons in various elements and chemical compounds. *Atomic Data*, 4:1, 1972.

[3] PIF. Paul Scherrer Institute Accelerator Facility, Users' Guide. Technical report, NSSDC WDC–A–R&S 76–06, NASA–GSFC, 1976.

[4] Ljungfelt, S. Calibration of STRV–REM. PSI internal report, 1994.

[5] Ljungfelt, S. Calibration of the MIR–REM ate the Proton Irradiation Facility of PSI with protons in the range 30 – 300 MeV. PSI internal report, 1994.

[6] Hajdas, W., Ljungfelt, S., and Cordt, I. Tests of the REM on the Betatron. *Paul Scherrer Institute, Annual Report*, FB3:155, 1994.

[7] GEANT. GEANT, detector description and simulation tool. Technical report, CERN Program Library Long Writeups W5013, 1993.

[8] Ljungfelt, S. Software simulation of the REM instrument. PSI internal report, in preparation, 1995.

[9] Lawson, C.L. and Hanson, R.J. *Solving least squares problems*. Prentice–Hall, 1974.

[10] Wells, N. The Space Technology Research Vehicles STRV–1A and STRV–1B: First in–orbit results. In *8th annual AIAA/Utha State University Conference on small satellites*, 1994.

[11] Wrenn, G.L. and Sims, A.J. Technology demonstration experiments on STRV–1. In *AGARD Flight Mechanics Panel:Space systems design and development testing Symposium, Cannes, France*, 1994.

[12] McIlwain, C.E. Coordinates for mapping the distribution of magnetically trapped particles. *Journal of Geophysical Research*, 66:3681, 1961.

[13] Sawyer, D.M. and Vette, J.I. AP–8 trapped proton environment for solar maximum and solar minimum. Technical report, NSSDC WDC–A–R&S 76–06, NASA–GSFC, 1976.

[14] Vette, J.I. The AE–8 trapped electron model environment. Technical report, NSSDC WDC–A–R&S 91–24, NASA–GSFC, 1976.